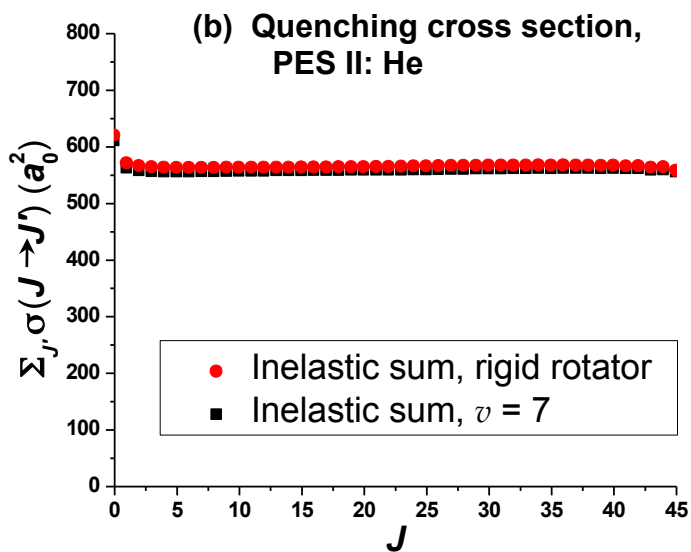
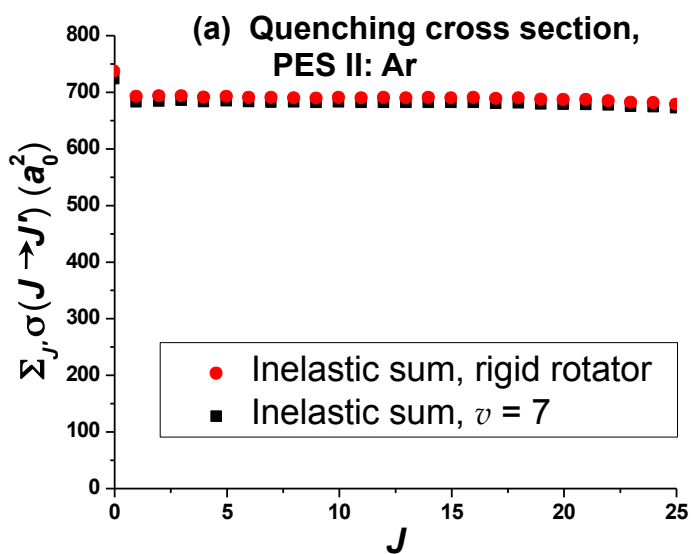
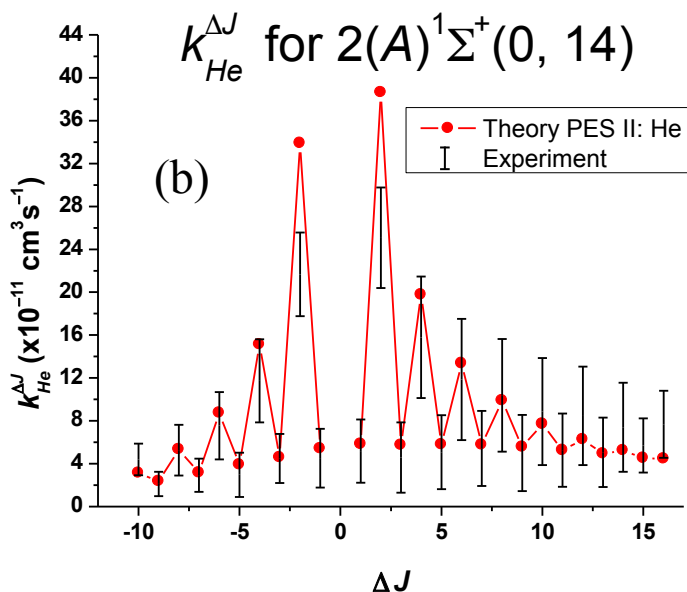
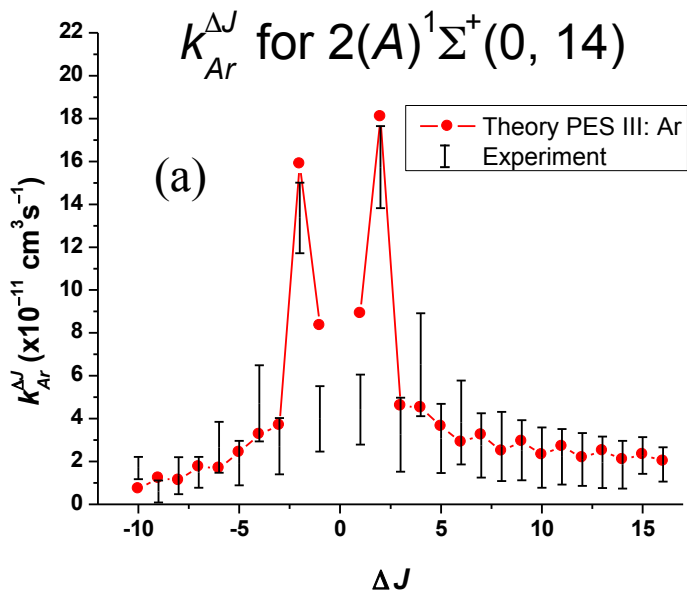


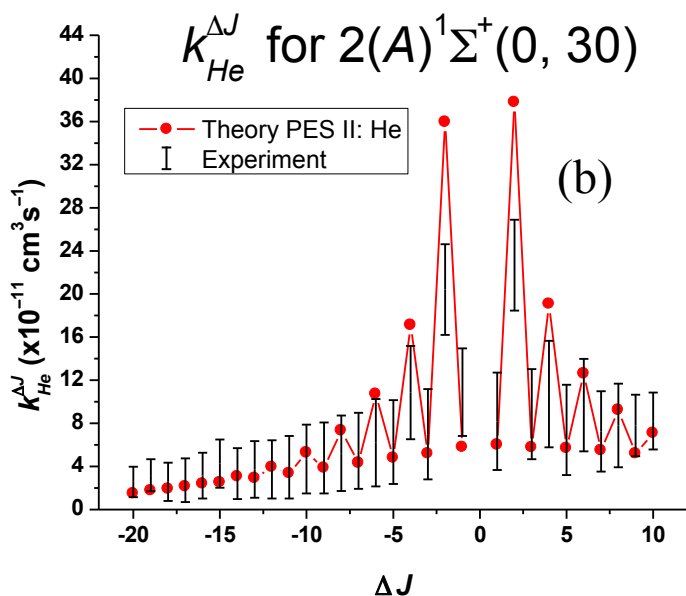
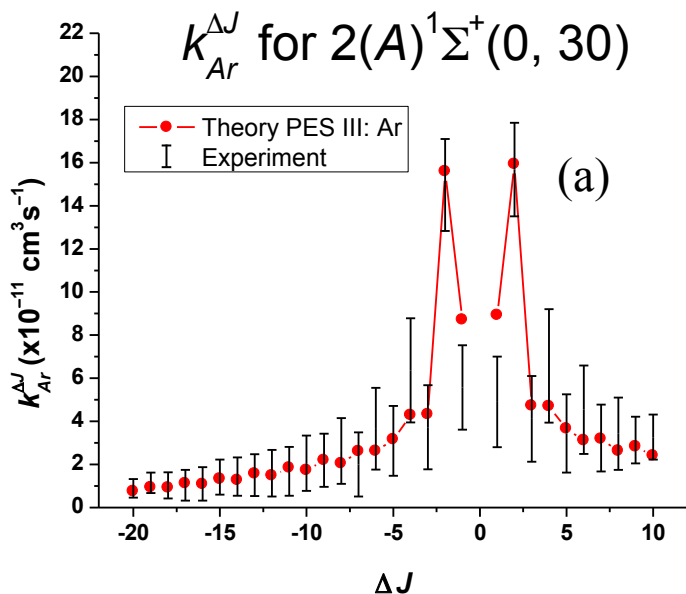
Supplementary Material Fig. 46. Sum of rotationally inelastic cross sections $\sum_{J' \neq J} \sigma(J \rightarrow J')$, as a function of initial J , for collisions of NaK $2(A)^1\Sigma^+(v=0, J)$ molecules, with (a) argon, and (b) helium perturbers. These results demonstrate that the quenching rates are mostly independent of rotational level. Initial J was limited to 45 in both cases to ensure that the sums had converged.



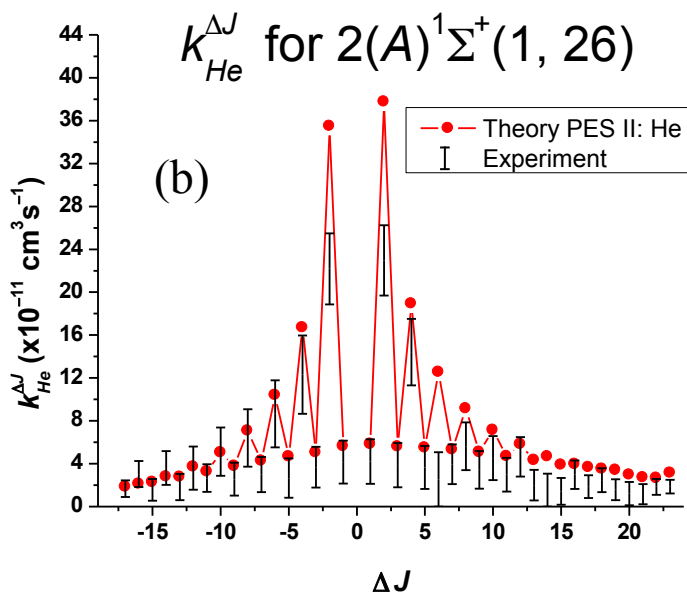
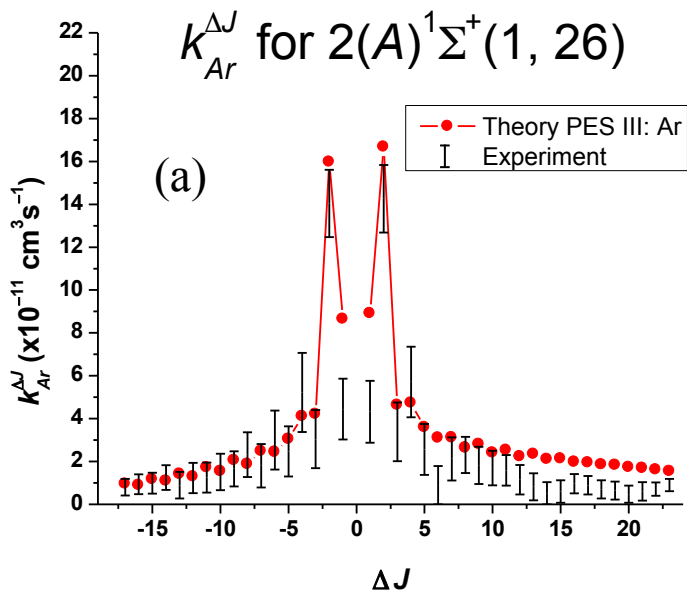
Supplementary Material Fig. 47. Sum of rotationally inelastic cross sections $\sum_{J' < J} \sigma(J \rightarrow J')$, as a function of initial J , for collisions of NaK $2(A)^1\Sigma^+(v, J)$ molecules, with (a) argon, and (b) helium perturbors. Red circles correspond to the rigid rotator, $v = 0$, and black squares correspond to $v = 7$, demonstrating that the quenching rates are mostly independent of vibrational level. Note that in part (a), the potential PES II: Ar was used to save computer time. Initial J was limited to 25 in part (a) and 45 in part (b) to ensure that the sums had converged.



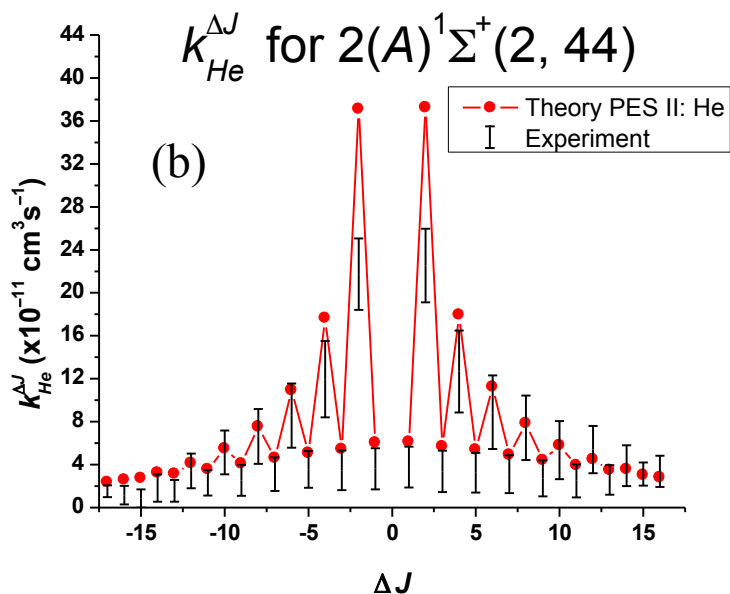
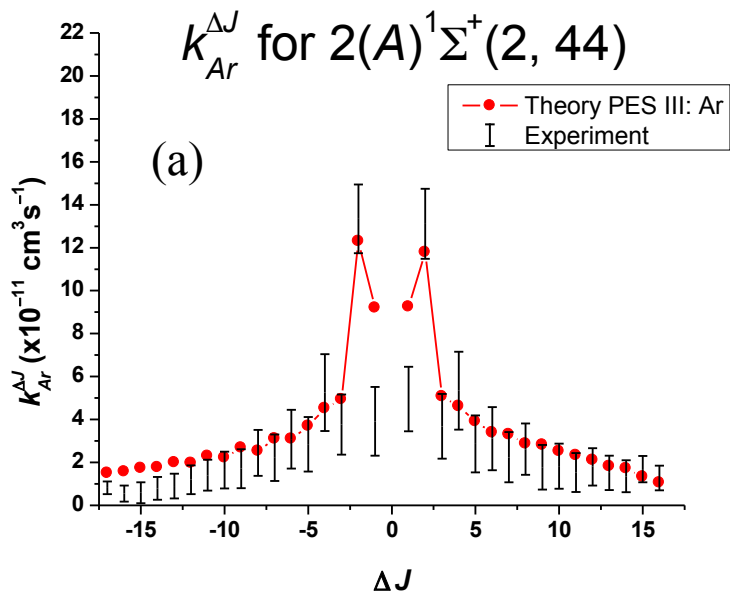
Supplementary Material Fig. 48. Approximate theoretical (rigid rotor) rate coefficients for rotationally inelastic collisions of NaK $2(A)^1\Sigma^+(v=0, J=14)$ molecules with (a) argon, and (b) helium, as functions of ΔJ , in comparison with experimental rate coefficients. The theoretical results for argon and helium were obtained using potential surfaces PES III: Ar and PES II: He, respectively. For comparison to experimental results, theoretical rate coefficients were obtained from calculated cross sections using the approximation $k_p^{\Delta J} = \langle \sigma_p^{\Delta J} \bar{v} \rangle \approx \sigma_p^{\Delta J} \bar{v}$. The upper limits of the experimental error bars are the upper limits of the “uncorrected” experimental rate coefficients shown in Fig. 8, while the lower limits of the experimental error bars are the rate coefficients corrected for multiple collision effects (see subsection 3 of the Appendix, Fig. 16a, and Supplementary Material Fig. 31).



Supplementary Material Fig. 49. Approximate theoretical (rigid rotor) rate coefficients for rotationally inelastic collisions of NaK $2(A)^1\Sigma^+(v=0, J=30)$ molecules with (a) argon, and (b) helium, as functions of ΔJ , in comparison with experimental rate coefficients. The theoretical results for argon and helium were obtained using potential surfaces PES III: Ar and PES II: He, respectively. For comparison to experimental results, theoretical rate coefficients were obtained from calculated cross sections using the approximation $k_p^{\Delta J} = \langle \sigma_p^{\Delta J} v \rangle \approx \sigma_p^{\Delta J} \bar{v}$. The upper limits of the experimental error bars are the upper limits of the “uncorrected” experimental rate coefficients shown in Fig. 28 of the Supplementary Material, while the lower limits of the experimental error bars are the rate coefficients corrected for multiple collision effects (see subsection 3 of the Appendix and Fig. 32 of the Supplementary Materials).

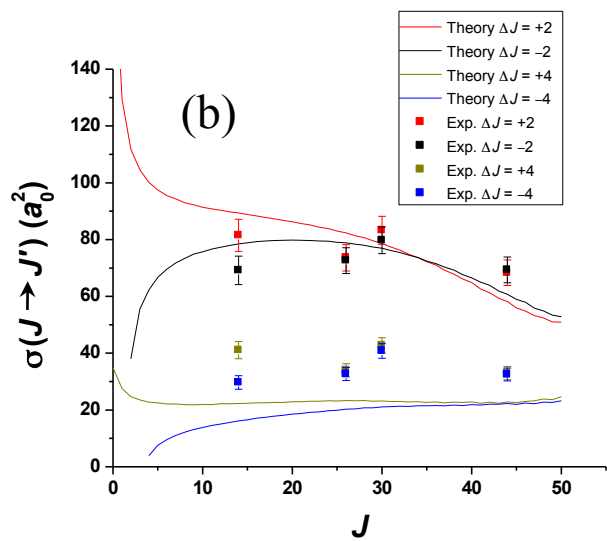
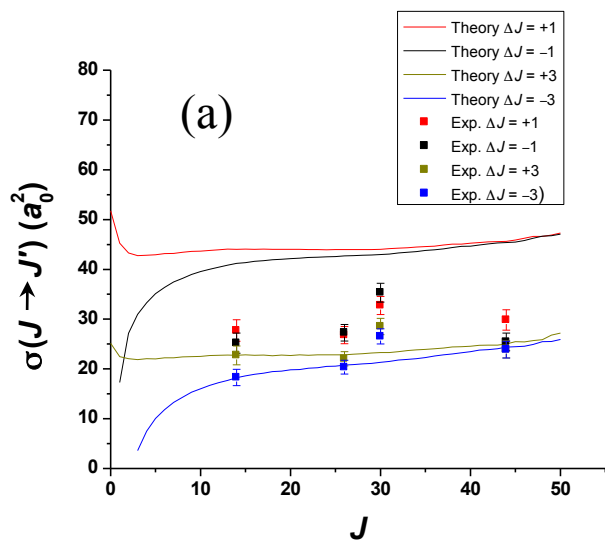


Supplementary Material Fig. 50. Approximate theoretical (rigid rotor) rate coefficients for rotationally inelastic collisions of NaK $2(A)^1\Sigma^+(v=1, J=26)$ molecules with (a) argon, and (b) helium, as functions of ΔJ , in comparison with experimental rate coefficients. The theoretical results for argon and helium were obtained using potential surfaces PES III: Ar and PES II: He, respectively. For comparison to experimental results, theoretical rate coefficients were obtained from calculated cross sections using the approximation $k_p^{\Delta J} = \langle \sigma_p^{\Delta J} v \rangle \approx \sigma_p^{\Delta J} \bar{v}$. The upper limits of the experimental error bars are the upper limits of the “uncorrected” experimental rate coefficients shown in Fig. 9, while the lower limits of the experimental error bars are the rate coefficients corrected for multiple collision effects (see subsection 3 of the Appendix and Fig. 33 of the Supplementary Material).

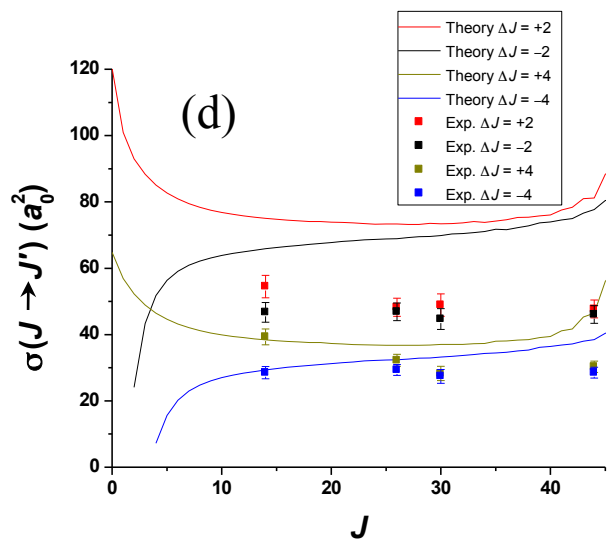
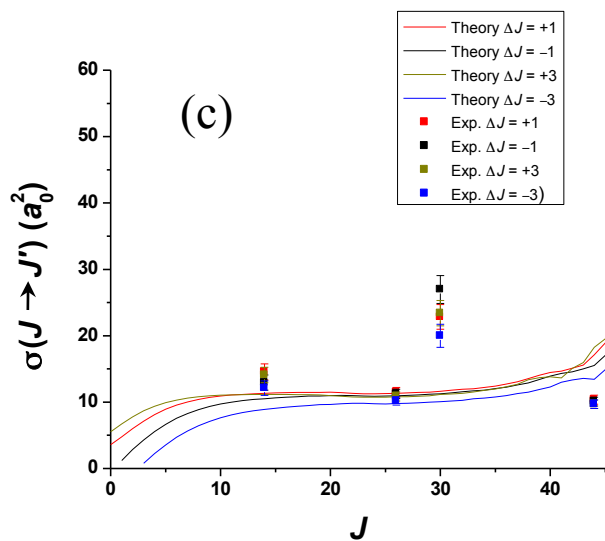


Supplementary Material Fig. 51. Approximate theoretical (rigid rotor) rate coefficients for rotationally inelastic collisions of NaK $2(A)^1\Sigma^+(v=2, J=44)$ molecules with (a) argon, and (b) helium, as functions of ΔJ , in comparison with experimental rate coefficients. The theoretical results for argon and helium were obtained using potential surfaces PES III: Ar and PES II: He, respectively. For comparison to experimental results, theoretical rate coefficients were obtained from calculated cross sections using the approximation $k_p^{\Delta J} = \langle \sigma_p^{\Delta J} v \rangle \approx \sigma_p^{\Delta J} \bar{v}$. The upper limits of the experimental error bars are the upper limits of the “uncorrected” experimental rate coefficients shown in Fig. 10, while the lower limits of the experimental error bars are the rate coefficients corrected for multiple collision effects (see subsection 3 of the Appendix Section C, Fig. 16b, and Supplementary Material Fig. 34).

Ar + NaK, PES III: Ar

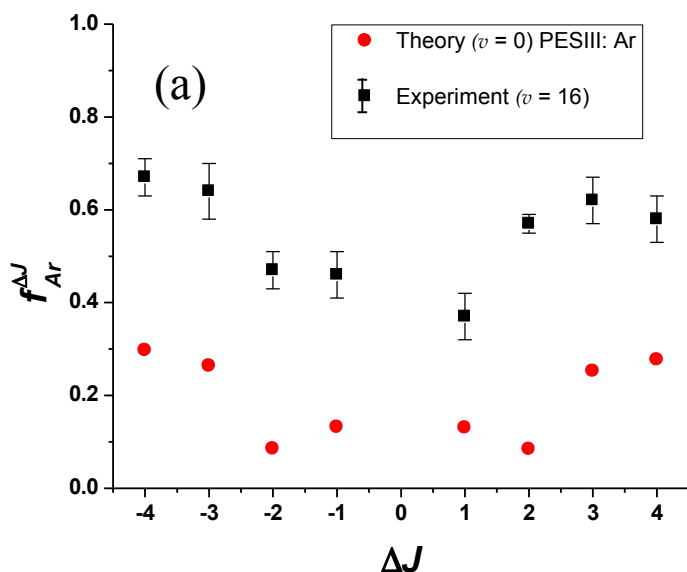


He + NaK, PES II: He

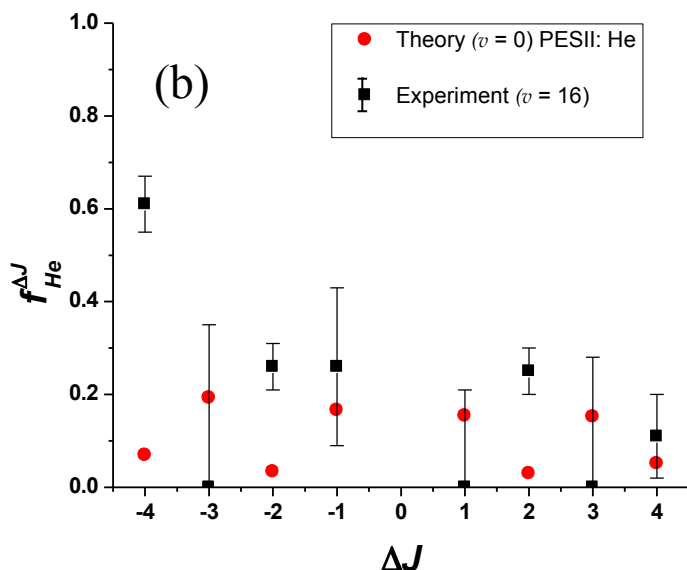


Supplementary Material Fig. 52. Cross sections in units of a_0^2 as a function of initial J for fixed ΔJ for (a) Ar + NaK, $\Delta J = \text{odd}$, (b) Ar + NaK, $\Delta J = \text{even}$, (c) He + NaK, $\Delta J = \text{odd}$, (d) He + NaK, $\Delta J = \text{even}$. Note that the predicted difference between positive and negative ΔJ is more pronounced at low J , and is generally consistent with the experimental data. Also note that for He + NaK, the odd and even transitions show qualitatively different behavior.

Ar + NaK, initial $J = 30$



He + NaK, initial $J = 30$



Supplementary Material Fig. 53. Comparison between theory and experiment of the fraction of orientation destroyed in rotationally inelastic collisions of NaK $2(A)^1\Sigma^+$ molecules with (a) argon and (b) helium atoms, as a function of ΔJ , for initial $J = 30$. The experimental data, corresponding to NaK $2(A)^1\Sigma^+(v = 16)$, are shown as black squares with error bars. The theoretical results, corresponding to NaK $2(A)^1\Sigma^+(v = 0)$, are shown as red circles.